Study on a cascaded DC-DC converter for use in Building-Integrated Photovoltaics

S. Ravyts*, M. Dalla Vecchia*, J. Zwysen*, G. Van den Broeck* and J. Driesen*
*KU Leuven - Department of Electrical Engineering (ESAT) - Electrical Energy and Computer Architectures (ELECTA)
EnergyVille - Thor Park 8301, 3600 Genk, Belgium
simon.ravyts@kuleuven.be

***Abstract*—In this paper, a two-stage power-electronics topology is presented for use in a BIPV module-level converter, connected to a low-voltage DC microgrid. The converter is built up as a cascade of two topologies, being an interleaved boost converter and a phase-shifted full bridge. The interleaved boost converter was chosen to lower the current stresses for the components and to reduce the required input and output capacitance due to the ripple current cancellation in the in- and output. The full bridge is chosen for its galvanic isolation and to perform the high step-up via the transformer turns ratio. It is shown that the maximum intermediate voltage level in between both converters can be derived from the continuous conduction mode of operation. Simulations are provided that show the correct operation of the overall structure. An experimental prototype has been built to demonstrate the overall performance of the converter.**

I. Introduction

The Strategic Energy Technology (SET) Plan [1] of the European Commision (EC) aims to reduce the emissions of carbon by encouraging the use of alternative energy sources. Specific implementation of the SET-Plan in the building sector has lead to a new legislation for buildings. By the end of 2018, all new buildings of public authorities need to be near-Zero-Energy-Buildings (nZEB), while by the end of 2020 all new buildings need to be nZEB. Near-Zero-Energy-Buildings are constructed in a way that their energy consumption is very low compared to traditional buildings, and the required energy is mainly produced locally via renewable sources [2].

Building Integrated PhotoVoltaics (BIPV), applied in the façade of the building seem to be a very attractive solution to enable the required targets and is also stimulated by the EC. This technology tries to integrate the PV panels inside other building elements such that multiple functions can be combined. In this specific case, a façade, offering protection against external influences is combined with an energy-generating device. Due to the non-ideal orientation of the PV panels to the sun and the possibility of partial shading due to other buildings or entities near the building, a module-level converter is often set forward as a better solution compared to the more traditional string inverter where arrays of PV panels are connected in series or in parallel [3].

978-1-5386-1006-0/18/$31.00

To further enhance the full potential of BIPV, integrating it into a DC microgrid offers several advantages compared to AC microgrids. The first one being that less copper is required to transfer the same amount of power in a DC grid. A second advantage is that less conversion steps are required to convert the DC power produced by the panels. This leads to higher overall system efficiency, higher reliability and simplifies the control. A third advantage is that the interchanging power with other DC appliances, such as energy storage devices, is also more efficient which can lead to significant energy savings in commercial and residential buildings [4].

The system of interest is shown in Fig. 1. Three parts can be distinguished: the PV panel, the DC grid and the module-level converter connecting both aformentioned parts. Notice that the module-level converter is an integrated part of the BIPV module and leads to an additional feature, which is the conditioning of the uncontrolled PV-generated power. The module-level converter only injects power to the DC grid and does not control this voltage level. This is usually done in a centralized AC/DC converter as described in [5].

This paper is constitued as follows: In section II, the specific challenges for BIPV converters are discussed. From these requirements, section III proposes a circuit topology that covers these aspects and section IV describes the chosen component values. Section V describes the dynamics of this converter and shows the simulation results. Section VI discusses the experimental prototypes and section VII presents the conclusion.

II. Design targets and challenges of BIPV converters

This section will describe the specific challenges that are related to converters intended for use in BIPV applications.

- **High compactness**: One of the targets for BIPV is to place the converter inside the framework of the module, such that it becomes an integrated part of the BIPV module. Mainly the height is a restricting

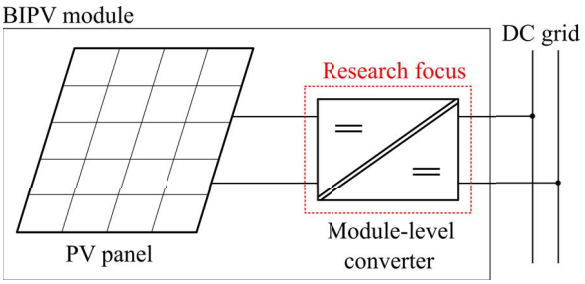

Fig. 1. Schematic overview of a BIPV module

factor: the total height (including casing) cannot exceed 40 mm to fit inside the framework.

- **Long lifetime**: The drawback of placing the converter in the aformementioned cavity is that the converter is difficult to reach and replacement after a failure is thus not an option. The system thus needs to be considered as non-repairable. From [6], where temperature sensors were placed in and around such a module, the maximum temperature is assumed to be 80°C. This relatively high temperature and associated temperature swings are important stress factors that wil shorten the lifetime of the components [7]. The targeted lifetime of the converter should be at least equal to 25 years, which is the current state-of-the-art lifetime for regular PV panels.
- **Cooling**: Active cooling via forced convection (e.g. by using a fan) cannot be implemented as the lifetime of the fan is too limited due to its rotating parts [8]. Liquid cooling is consided to be too expensive and difficult to implement. The only viable alternative seems to be a passive cooling method using a heat-sink. It is however important that the physical dimensions of the heat-sink are still compatible with the high compactness criterion defined previously. In [6], temperatures are measured on several BIPV test panels. The maximum temperature can vary in between 60 to 100°C, measured at different locations on the PV panel. From these measurements, the ambient temperature for the converter is expected to be in the same range, depending on the exact placement.
- **Plug-and-play**: To reduce both the installation costs and the engineering effort that is required to design the BIPV installation, a plug-and-play solution is preferred. This means that all BIPV modules are connected in parallel to the common DC bus.
- **Wide operating range**: To be able to use the converter for different types of PV panels (mono, poly or amorph cristalline), with their respective I-V characteristics, the converter needs to be able to work for a wide variety of voltages and currents. Next to the ability to work with different types of PV panels, this also enables to harvest the solar energy on instances with limited solar irradiation and thus low input power. This wide operating range can also be seen from the converter specifications given in Table I.
- **High static gain**: The voltage level of the DC grid is chosen to be +380V. The output voltage of the PV panel can be as low as 10V due to low solar irradiation, non-ideal orientation to the sun or the choice to make a PV panel with less cells. As a consequence, the gain of the converter needs to be as high as 38 under several circumstances. This high gain might lead to lower conversion efficiencies as discussed in [9].
- **Galvanic isolation**: For safety reasons and a maximum compatibility to every type of DC grid, galvanic isolation between the PV panel and the DC grid is deemed necessary.

TABLE I
CONVERTER SPECIFICATIONS

Parameter	Value
V_{in}	10-50 V
V_{out}	380 V
I_{in}	1-10 A
P_{max}	300 W

Another aspect, which holds for all PV converters, is that the input current ripple needs to be small. A high current ripple causes oscillations around the MPP, which leads to a lower overall efficiency [10]. The electrical requirements are listed in Table I.

III. Choice of topology

From the above discussion and the requirements of Table I, a cascade of an interleaved Boost converter and a voltage-fed full bridge converter has been chosen and is shown in Fig. 2. The two converters are treated separately below.

A. Interleaved Boost Converter

A boost converter, operating in Continuous Conduction Mode (CCM), is chosen as the primary stage, which increases the voltage to an intermediate voltage level Vm. This topology is chosen because it has an inductor at the input, limiting the current ripple and because it is easy to parallelize. The latter can be used to further decrease the input current ripple when several (N) boost converters operate interleaved, with a phase-shift of 360°/N. Applying this methodology, the current stresses across the power semiconductors is divided equally, which enables the use of components with lower current ratings and, consequently, lower on-resistances which reduce the conduction losses, increasing the overall efficiency of the system. Fig. 3 shows the reduction in the ripple current, normalized with respect to the ripple in a single (N=1) boost converter, given by (1), where δ_b represents the duty cycle of the interleaved Boost converter and $f_{s,b}$

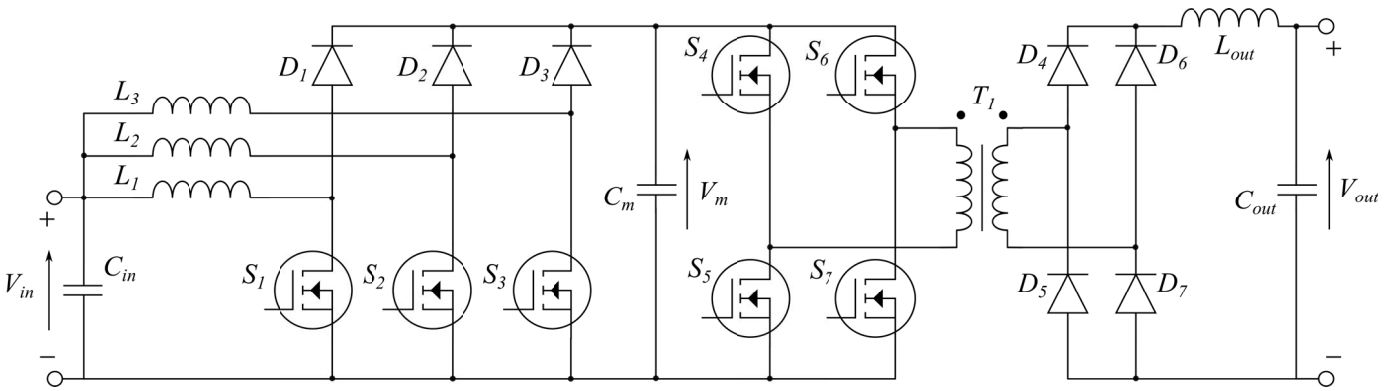

Fig. 2. Cascade of a Boost and a full bridge converter

represents the switching frequency . A second advantage of the interleaving is that the input- and output capacitors can be chosen smaller, which leads to smaller dimensions of the board.

$$\Delta I = \frac{V_{in}.\delta_b}{L.f_{s,b}} \tag{1}$$

Three interleaved legs (N=3) are chosen for this application as standard SMD components (inductors, switches and diodes) are available in this current range ($I_{in}/3 = 3,33A$). Besides, the mean input voltage is expected to be around 30 V and the intermediate DC bus voltage is will be around 100 V. The duty cycle that corresponds to this gain ($\delta_b = 0.70$) is very close to $\delta_b = 0.67$, one of the two points where an entire cancellation is achieved in a three-legs interleaved Boost.

The possibility of redundant operation is a third major advantage of the interleaved structure. In case of an (open-circuit) failure of one of the components, the converter can remain operational with the other two legs [11].

To achieve a higher efficiency below the nominal operation point, one or more phases can be disabled such that the power is processed by only one or two legs instead of all three legs together [12]. Next to a higher overall efficiency, the Boost converter will operate over a wider range in CCM, which leads to a simpler control strategy. This last point is a fourth advantage that increases the operation range of the converter.

B. Full Bridge Converter

The second stage is a voltage-fed phase-shifted full bridge converter as it is known to achieve a high gain, galvanic isolation and a high efficiency. The bi-directional core excitation allows to reduce the physical dimensions of the transformer, leading to a higher power density compared to converters with a uni-directional core-excitation such as a Flyback. Note that the output of the transformer is connected a diode bridge rectifier and an LC filter. The diode bridge topology was preferred above the full-wave rectifier. Despite the higher amount of diodes (4 instead of 2) and thus higher conduction losses, the transformer does not require a center-tap and the breakdown voltage of the diodes can be chosen lower. This is beneficial given the relatively high DC bus voltage (+380 V) and thus leads to a higher reliability and lower costs.

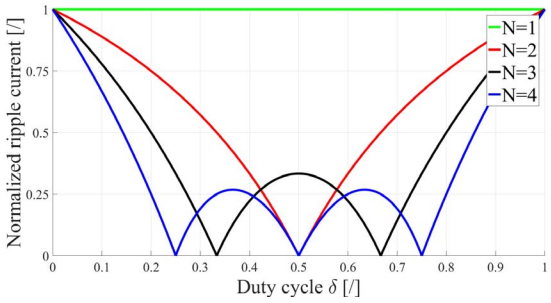

Fig. 3. Normalized ripple current of an interleaved Boost converter

The ripple in the output inductor L_{out} is given by (2), where n represents the transformer turns ratio, δ_{fb} represents the duty cycle and V_m represents the input voltage of the full bridge. If one wants the full bridge to operate over the entire operating area in CCM, L_{out} needs to be chosen very large. This would lead to bigger physical dimensions and possibly a lower efficiency due to high copper losses (more windings). Therefore, the full bridge will be designed in a way that it operates under CCM or DCM, depending on the instant power level of the converter.

$$\Delta I_{L,out} = \frac{(n.V_m - V_{out}).\delta_{fb}}{2.L_{out}.f_s} \tag{2}$$

IV. Component selection

In this section, the sizing and selection of the components will be discussed. The focus will be on the reliability, compactness and temperature influence.

A. Capacitors

Electrolytic capacitors seem interesting to use as they have the highest capacitance per volume (C/V) ratio,

TABLE II
COMPONENTS OF THE CASCADED CONVERTER

Designator	Value	Type
$f_{s,b}$	200 kHz	-
$f_{s,fb}$	100 kHz	-
C_{in}	6 μF	B32529D1105J000
C_m	10 μF	B32522N3105K000
C_{out}	6 μF	B32672P5105K000
$L_1 - L_3$	100 μH	SRP1770TA-101M
L_{out}	330 μH	MSS1278T-334KL
$S_1 - S_7$	Si MOSFET	IPB320N20N3
$D_1 - D_3$	Si diode	VS10CSH02HM3
$D_4 - D_7$	Si diode	RS2K

which can help to achieve a high power density for the converter. However, reliability studies have shown that temperature is one of the main aging factors for power electronic components such as switching devices and capacitors [7], [13]. Mainly electrolytic capacitors tend to fail within short periods, e.g. ten years [14]. To prolong the lifetime of the converter, a circuit without electrolytic capacitors is thus preferred. To fulfill this requirement, the switching frequency needs to be chosen high enough such that film or ceramic capacitors (with a lower C/V ratio) can be used in the design.

B. Inductors and transformer

A high switching frequency is beneficial for the required input inductors as well. From (1), the required inductance for a certain current ripple decreases with the switching frequency. Also the physical dimensions of the transformer will be lower for higher switching frequencies.

C. Switches and diodes

To enable the high compactness requirement, SMD MOSFETs and diodes are chosen for this converter. An added advantage for these components is that the heatsink can be implemented on the PCB via a large copper area, increasing again the power density.

The chosen components are given in Table II.

V. CONTROLLER IMPLEMENTATION AND DESIGN

A. Boost Converter

The transfer function of a single Boost converter is desribed by [15]:

$$\frac{i_L(s)}{\delta(s)} = \frac{C_m.V_{out}.s + 2(1-\delta_b).I_L}{L.C.s^2 + (L/R).s + (1-\delta_b)^2} \quad (3)$$

In this equation, the full bridge is approximated as an equivalent loading resistance, R. A first-order PI controller was designed with a crossover frequency of 4 kHz and a Phase Margin (PM) of 70° to have sufficient damping in the system. After further fine-tuning, satisfactory controller parameters were found to be $K_p = 0.1$ and $K_i = 80$.

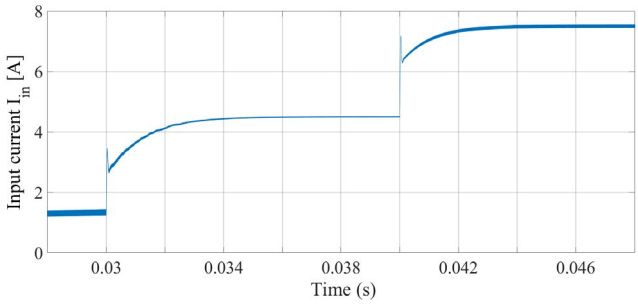

Fig. 4. Step response of the input current of the converter

The system's response for a load step from 1.5 A to 4.5 A to 7.5 A is shown in Fig. 4.

B. Full Bridge Converter

As previously mentioned in section III-B, the output inductance needs to be very large when the converter needs to operate in CCM over the entire operating range. Therefore, the full bridge will operate under DCM for lower input powers.

Under CCM, the transfer function of the phase-shifted full bridge is given by:

$$V_{out} = V_m.n.\delta_{fb} \quad (4)$$

Since V_{out} will be controlled by an external converter, as discussed in [5], (4) can be used to control V_m, which is the voltage in between the Boost and the full bridge. This voltage however does not need to be regulated very precisely as it is only an intermediate stage and it is thus chosen to regulate it in open-loop. The most important is that there are no over-voltages that can destroy the capacitors or the switches. For example, with $V_{out} = 380$V, $V_m = 100$V and n = 5.5, the duty cycle can be set to 69%. It is however important that under DCM, the same open-loop control strategy can be maintained. Under DCM, one can destinguish three intervals in the current waveform, shown in Fig. 5. During δ, i_L will rise, during δ', i_L will decrease and during δ'', $i_L = 0$. From the output inductor volt-second balance, one can find:

$$V_m = \frac{V_{out}.(\delta_{fb} + \delta'_{fb})}{n.\delta_{fb}} \quad (5)$$

and since

$$\delta_{fb} + \delta'_{fb} + \delta''_{fb} = 1 \quad (6)$$

one can be certain that V_m will always be lower under DCM. The maximum voltage stress on the intermediate capacitor will thus occur under CCM. To determine V_m, one can rewrite the previous equation for δ' and fill this in in the equation for the average current through L_{out}, which is related to the average output power P_{out}. A quadratic equation in V_m is found, where only the positive result is valid:

$$n^2.\delta_{fb}.V_m^2 - n.V_{out}.\delta_{fb}.V_m - \frac{4.I_L.V_{out}.L.f_s}{\delta_{fb}} = 0 \quad (7)$$

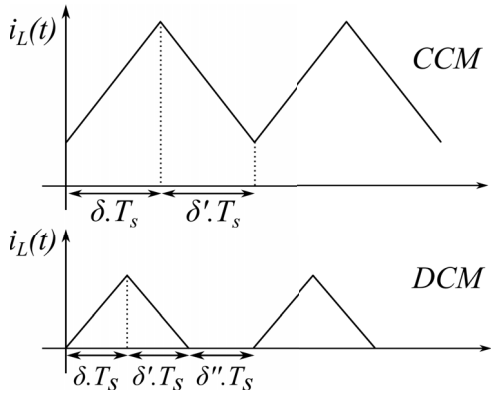

Fig. 5. Definition of δ, δ' and δ"

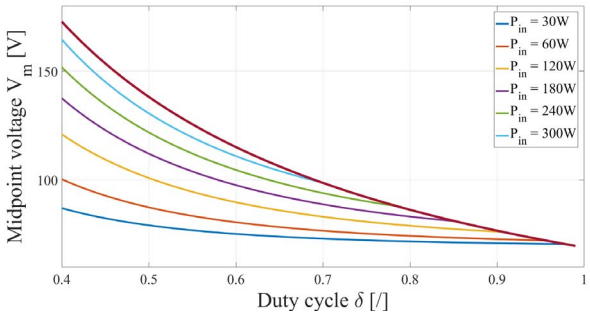

Fig. 6. Midpoint voltage V_m as a function of duty cycle and power

The result of this analysis is shown in Fig. 6 where V_m as a function of δ_{fb} is plotted for different input powers. The top (red) line corresponds with CCM and lower lines correspond to DCM. Under CCM, V_m is solely determined by the duty cycle, while under DCM, both the duty cycle and the input power from the PV panel will determine the midpoint voltage V_m. Fig. 7 shows the measured V_m for different power steps in the PLECS simulation environment. It can be seen that this simulation result corresponds closely to the results obtained via (7). Without closed-loop control, the midpoint voltage V_m will increase with increasing power level. When the converter reaches CCM, the voltage will remain constant and is determined by the chosen duty cycle. In this simulation, the duty cycle was set to 70 %, as the maximum V_m will then be around 100V and the converter will operate on the border between CCM and DCM. Note that the transients during a change in power are fast and without overshoot.

VI. Experimental results

Both the interleaved Boost converter and the phase-shifted full bridge have been designed on a PCB. Pictures of the first prototypes are shown in Figs. 8a and 8b. The efficiency plot of the interleaved Boost converter, where the input voltage is varied from 10-50 V and the output voltage is kept constant at 100 V, is shown in Fig. 9. It can be seen that the overall efficiency drops for lower

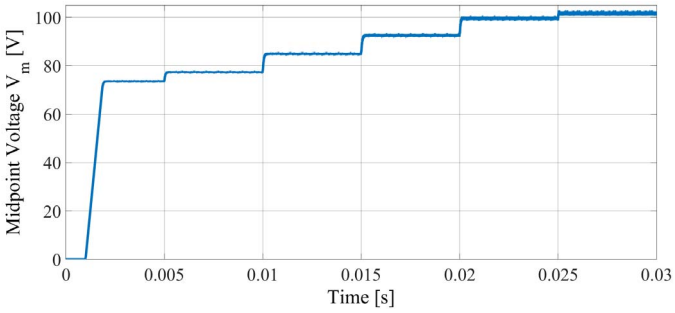

Fig. 7. Midpoint voltage as a function of time when the PV-generated power increases stepwise

input voltages, corresponding to higher duty cycles. A peak efficiency of 96,6 % is obtained. An efficiency plot of the full bridge could however not be obtained due to high voltage overshoots on the secondary side of the transformer, leading to extra losses in the output diodes and the output inductor. A measurement of the transformer primary voltage (green), the transformer secondary voltage (purple) and the current through L_{out} (yellow) is shown in Fig. 10. This phenomenon is probably due to a resonant behaviour between the secondary stray inductance and the intra-winding capacitance of the transformer.

VII. Conclusion

First, several challenging aspects for BIPV converters such as long lifetime, high compactness, high gain and a wide operating range have been discussed. Then a converter design was proposed and the components were selected. The control strategy of the converter is partly closed-loop, partly open-loop. The interleaved Boost converter stage, which will take care of the MPPT and works always under CCM is controlled in closed loop. The second stage, a phase-shifted full bridge, can work under both CCM or DCM. The control of this stage is purely open loop and it has been shown that the voltage stresses can be derived from CCM, as the voltage stress under DCM will always be lower. Finally, PCB prototypes of the Boost and the full bridge converter were developed. The Boost converter works as expected and achieves good efficiencies. However, the full bridge secondary has to deal with oscillatory behaviour and as a consequence, it was not possible to measure the efficiency curve as it was not possible to use the converter under nominal operating conditions. Further research is needed to come up with a good solution for this problem.

Acknowledgment

This research has been carried out in the framework of the EFRO SALK Solsthore project.

References

[1] European Commision, "Towards an Integrated Strategic Energy Technology (SET) Plan: Accelerating the European Energy System Transformation," 2015.

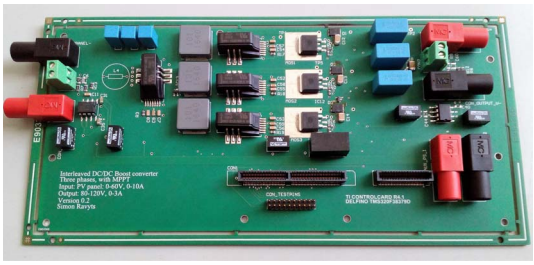

(a) Boost converter (115 x 250 x 30 mm^3)

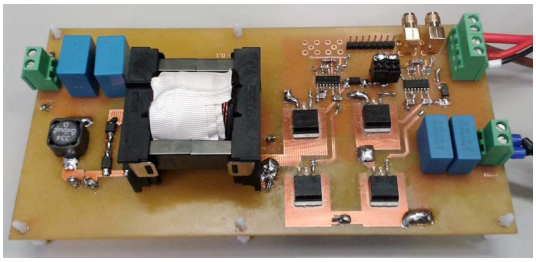

(b) Full bridge converter (90 x 170 x 50 mm^3)

Fig. 8. PCB prototypes of the converter

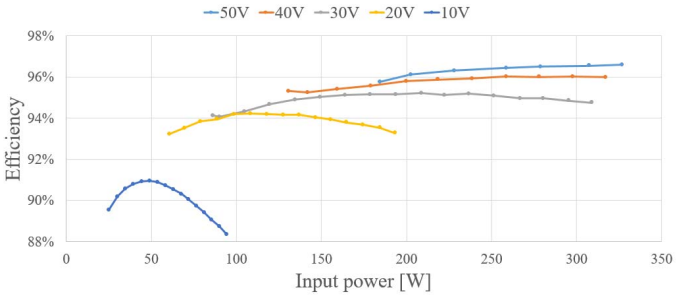

Fig. 9. Efficiency curves of the Boost converter for different input voltages and a fixed output voltage of 100 V and a switching frequency of 100 kHz

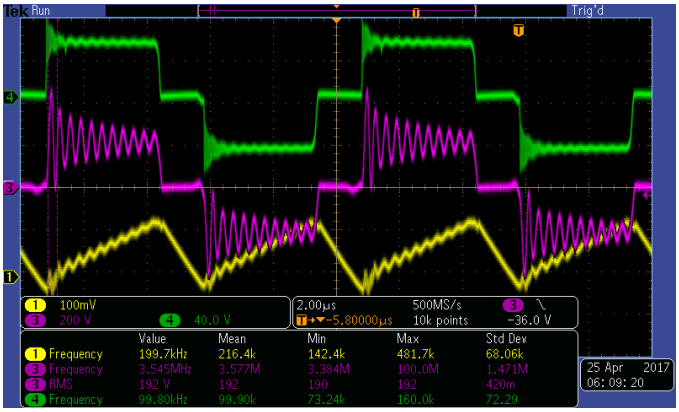

Fig. 10. Measurement of the primary voltage (green), secondary voltage (purple) and output inductor current (yellow) of the full bridge converter

[2] EU, "Directive 2010/31/EU of the European Parliament and of the Council of 19 May 2010 on the energy performance of buildings (recast)," *Official Journal of the European Union*, pp. 13–35, 2010.

[3] U. Chatterjee, R. Gelagaev, A. Masolin, and J. Driesen, "Design of an intra-module DC-DC converter for PV application: Design considerations and prototype," *IECON Proceedings (Industrial Electronics Conference)*, pp. 2017–2022, 2014.

[4] J. J. Justo, F. Mwasilu, J. Lee, and J. W. Jung, "AC-microgrids versus DC-microgrids with distributed energy resources: A review," *Renewable and Sustainable Energy Reviews*, vol. 24, pp. 387–405, 2013.

[5] T. Dragi and J. M. Guerrero, "DC Microgrids Part II : A Review of Power Architectures , Applications , and Standardization Issues," *IEEE Transactions on Power Electronics*, vol. 31, no. 5, pp. 3528–3549, 2016.

[6] G. V. D. Broeck, W. Parys, H. Goverde, S. V. D. Putten, J. Poortmans, J. Driesen, and K. Baert, "Experimental analysis of the performance of facade-integrated BIPV in different configurations," in *32nd European Photovoltaic Solar Energy Conference and Exhibition*, Munich, 2016, pp. 1–5.

[7] H. Wang, K. Ma, and F. Blaabjerg, "Design for reliability of power electronic systems," in *IECON 2012 - 38th Annual Conference on IEEE Industrial Electronics Society*, 2012, pp. 33–44.

[8] X. Tian, "Cooling fan reliability: Failure criteria, accelerated life testing, modeling and qualification," *Proceedings - Annual Reliability and Maintainability Symposium*, vol. 00, no. C, pp. 380–384, 2006.

[9] W. Josias de Paula, D. d. S. Oliveira Junior, D. d. C. Pereira, and F. L. Tofoli, "Survey on non-isolated high-voltage step-up dcâĂŞdc topologies based on the boost converter," *IET Power Electronics*, vol. 8, no. 10, pp. 2044–2057, 2015.

[10] J. Flicker, R. Kaplar, M. Marinella, and J. Granata, "PV Inverter Performance and Reliability: What is the Role of the Bus Capacitor?" *PhotoVoltaic Specialists Conference (PVSC)*, vol. 2, pp. 2–4, 2012.

[11] F. H. Aghdam and M. Abapour, "Reliability and Cost Analysis of Multistage Boost Converters Connected to PV Panels," *IEEE Journal of Photovoltaics*, vol. 6, no. 4, pp. 981–989, 2016.

[12] V. Michal, "Optimal peak-efficiency control of the CMOS interleaved multi-phase step-down DC-DC Converter with segmented power stage," *IET Power Electronics*, vol. 9, no. 11, pp. 2223–2228, 2016.

[13] K. Ma, M. Liserre, and F. Blaabjerg, "Lifetime estimation for the power semiconductors considering mission profiles in wind power converter," *2013 IEEE Energy Conversion Congress and Exposition, ECCE 2013*, pp. 2962–2971, 2013.

[14] H. Wang and F. Blaabjerg, "Reliability of capacitors for DC-link applications in power electronic convertersâĂŤan overview," *IEEE Transactions on Industry Applications*, vol. 50, no. 5, pp. 3569–3578, 2014.

[15] S. Kolluri and N. L. Narasamma, "Analysis, modeling, design and implementation of average current mode control for interleaved boost converter," *2013 IEEE 10th International Conference on Power Electronics and Drive Systems (PEDS)*, no. 4, pp. 280–285, 2013.